


Article

Influence of Golden Nanoparticles on the Incorporation of Eu^{2+} into BaI_2 and Defect Concentration

Katarína Ridzoňová^{1,2}, Maksym Buryi^{1,3,*} , Vladimír Babin¹, David John^{1,3,4} , Jan Drahošoupil¹, Neda Neykova^{1,5} , Tatsiana Salamakha⁶ and Yauhen Tratsiak⁶

¹ FZU—Institute of Physics of the Czech Academy of Sciences, Na Slovance 1999/2, 18200 Prague, Czech Republic

² Faculty of Mathematics and Physics, Charles University, Ke Karlovu 2027/3, 12116 Prague, Czech Republic

³ Faculty of Nuclear Sciences and Physical Engineering, Czech Technical University, Břehová 7,

11519 Prague, Czech Republic

⁴ Nuclear Physics Institute of the Czech Academy of Sciences, Na Truhlářce 39/64, 18000 Prague, Czech Republic

⁵ Centre for Advanced Photovoltaics, Faculty for Electrical Engineering, Czech Technical University in Prague, Technická 2, 16627 Prague, Czech Republic

⁶ Research Institute for Physical Chemical Problems of the Belarusian State University, 220030 Minsk, Belarus

* Correspondence: buryi@fzu.cz

Abstract: Conjugated $\text{BaI}_2\text{:Eu}$ (5 at.%) nanocrystalline particles were synthesized, decorated with golden nanoparticles (GNP). GNP demonstrated some hydrophilic effect, leading to the $\text{BaI}_2\cdot\text{H}_2\text{O}$ phase creation. The Eu^{2+} luminescence intensity was reduced according to the GNP content. This was due to the decreased number of Eu^{2+} ions in the BaI_2 , most probably, arising from the Au substitution for Ba competing with Eu. Moreover, the decay time of luminescence was decreased upon GNP content. This was explained by the moderation of negative charge in the GNP, leading to the repulsion with an electron in the excited Eu^{2+} .

Keywords: barium iodide; Eu^{2+} , Au nanoparticles; luminescence; EPR



Citation: Ridzoňová, K.; Buryi, M.; Babin, V.; John, D.; Drahošoupil, J.; Neykova, N.; Salamakha, T.; Tratsiak, Y. Influence of Golden Nanoparticles on the Incorporation of Eu^{2+} into BaI_2 and Defect Concentration. *Crystals* **2023**, *13*, 902. <https://doi.org/10.3390/cryst13060902>

Academic Editor: Alessandro Chiasera

Received: 28 April 2023

Revised: 19 May 2023

Accepted: 24 May 2023

Published: 1 June 2023



Copyright: © 2023 by the authors. Licensee MDPI, Basel, Switzerland. This article is an open access article distributed under the terms and conditions of the Creative Commons Attribution (CC BY) license (<https://creativecommons.org/licenses/by/4.0/>).

1. Introduction

Development of effective scintillator materials with low-cost manufacturing still remains a current issue due to the absence of an ideal phosphor [1]. The alkaline-earth binary halides, such as CaI_2 , SrI_2 , BaCl_2 , BaBr_2 and BaI_2 , represent, thanks to their high effective atomic numbers ($Z \sim 50$), high light yields (up to 100,000 photon/MeV) and low-cost synthesis, making them promising materials for scintillation radiation detectors [2–7]. To enhance their luminescent properties, alkaline-earth halides require activation by a dopant. Rare earths ions, such as Eu^{2+} , Eu^{3+} , Ce^{3+} or Tb^{3+} are amongst the most-used dopants with their selection dependent on the required emission spectra [8]. Both charge states of europium, Eu^{2+} and Eu^{3+} , emit under UV irradiation in the visible spectral region. The exact luminescence efficiency and spectral region of the europium activator is dependent on the surrounding environment and on the $\text{Eu}^{2+}/\text{Eu}^{3+}$ ratio [9,10]. The Eu^{2+} dopant particularly emits in the blue region [11,12] thanks to $5d-4f$ transition, while Eu^{3+} ions have been shown to exhibit narrow emissions in the red, blue and green regions corresponding to $f-f$ transitions [11–16].

Barium iodide (BaI_2) may be considered as one of the most effective scintillation materials in the alkaline-earth halides family thanks to its relatively high atomic number ($Z = 54$) [17]. BaI_2 is additionally characterized by high light output (up to 60,000 photons/MeV), broad bandgap of 5 eV, sufficient density of $5.1 \text{ g}\cdot\text{cm}^{-3}$, absence of intrinsic radioactivity and is less hygroscopic compared to other alkali-earth halides [17,18]. Barium iodide may be grown in the form of orthorhombic single crystals by the Bridgman method [17]. However, due to the hygroscopic nature of most alkaline-earth halides and synthesis cost reduction, BaI_2 is more often synthesized in form of nanocrystals incorporated into the glass–ceramic matrix which act as protection from moisture in the air [8].

Eu^{2+} and Eu^{3+} ions represent a suitable activator for BaI_2 while their effect on structural, morphological and optoelectronic properties have been previously subjected to research in [18,19].

Besides using the dopant activator, the addition of nanoparticles may further significantly improve material optical properties [20–23]. In particular, the incorporation of Au ions into BaBrCl:Eu single crystals leads to the enhancement of photoluminescence intensity and reduces long afterglow. Similar improvement of luminescent properties has also been previously observed in Eu-activated germanate films with golden nanoparticles (GNPs) [24–26]. The co-doping with nanoparticles may also enable radiation absorption in other regions of the spectrum, while the exact absorption spectrum may be tuned by varying the size and surface morphology of the nanoparticles used [27,28]. The previously observed improvement of Eu^{2+} luminescent properties in alkaline-earth binary halides may originate in the formation of AuX , AuX_2^- and AuX_4^- halide compounds in BaX_2 where X stands for the halide used. Such halide compound formation leads to excess electron creation, which may be subsequently captured by Eu^{3+} —resulting in the increase of Eu^{2+} concentration and its PL luminescence [29]. Another possible explanation of GNPs-induced PL improvement may originate in the Richardson–Schottky effect coupled with the plasmonic Au nanoparticles [30,31]. The incident excitation light excites electrons in the golden nanoparticles which are then transferred to the conduction band of the $\text{BaX}_2:\text{Eu}$ particles. These excess electrons then contribute to the Eu^{2+} luminescence being relaxed from the conduction band appearing at the excited state of the Eu^{2+} with the subsequent recombination. The larger the amount of Au nanoparticles, the more the electrons appear in the BaX_2 . Lastly, the GNPs may suppress the number of non-radiative recombination centers in $\text{BaX}_2:\text{Eu}$.

Based on the previous successful implementation of GNPs into BaBrCl:Eu single crystals, the co-doping of $\text{BaI}_2:\text{Eu}$ microcrystalline powders with GNPs has been presently tested. To understand the exact effect of GNPs on $\text{BaI}_2:\text{Eu}$ properties, X-ray diffraction spectroscopy (XRD), photoluminescence (PL) spectroscopy, PL decay measurements, radioluminescence (RL) spectroscopy and electron paramagnetic resonance (EPR) spectroscopy have been combined in the present study. The influence of the varying GNP concentration on the incorporation of Eu^{2+} into the BaI_2 lattice and defect concentration were investigated as well.

2. Experimental

2.1. Preparation of $\text{BaI}_2:\text{Eu}$ Samples with GNPs

The following materials of analytical grade were used in the sample synthesis: $\text{Ba}(\text{NO}_3)_2$, NH_4I , $\text{Eu}(\text{NO}_3)_3 \cdot 6\text{H}_2\text{O}$, NH_4HCO_3 , NaOH , Na_2EDTA and HAuCl_4 . A two-stage process, described in more detail in [19,32], was used for $\text{BaI}_2:\text{Eu}$ powders synthesis. GNPs were added in the form of Au solution in the amount of 0, 0.01, 0.05 and 0.2 wt.% to the precursor $\text{BaCO}_3:\text{Eu}$ which was prepared during the first stage of synthesis.

To prepare GNPs, 0.075 mole/ dm^3 of NaOH was mixed under constant stirring into 0.008 mole/ dm^3 of Na_2EDTA to a pH level of 10.5. The resulting solution was gradually heated with a time step of ~ 2 °C/min and then 0.023 mole/ dm^3 of HAuCl_4 was added while keeping the mixture at 90 °C for another 30 min. Concentration of Au in the resulting mixture was 5×10^{-4} mole/ dm^3 .

To prepare $\text{BaCO}_3:\text{Eu}$ powder, 0.1 mole/ dm^3 of $\text{Eu}(\text{NO}_3)_3$ was mixed into 0.2 mole/ dm^3 of $\text{Ba}(\text{NO}_3)_2$. The chosen concentration of $\text{Eu}(\text{NO}_3)_3$ leads to 5 at.% replacement of Ba^{2+} ions by Eu^{3+} ions. The nitrate mixture was subsequently added under constant stirring into 1.2 mole/ dm^3 of NH_4HCO_3 . The obtained $\text{BaCO}_3:\text{Eu}$ precipitate was then centrifuged and rinsed by distilled water.

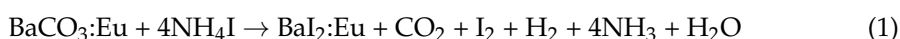
The required amounts of GNPs were calculated according to the weight of Ba in the samples and were added to $\text{BaCO}_3:\text{Eu}$ upon 1 h constant stirring. The obtained suspensions were annealed at 80 °C for 12 h and subsequently stirred for 10–15 min.

In the second stage, BaCO₃:Eu doped with GNPs was mixed with NH₄I powders and then annealed at 400 °C for 30 min under Ar flow. The samples were then left to cool to the room temperature under the Ar flow. The designations of the samples with their corresponding amounts of GNPs used in the sample preparation are listed in Table 1.

Table 1. Designations of the obtained samples varying in the used amount of GNPs.

| Sample | Au0 | Au001 | Au005 | Au02 |
|----------|-----|-------|-------|------|
| Au, wt.% | 0 | 0.01 | 0.05 | 0.2 |

The second stage of the sample preparation is governed by the following chemical equation:



2.2. Experimental Techniques

The samples were stored between individual measurements in the glovebox filled with Ar to prevent the interaction with atmosphere [8].

X-ray diffraction (XRD) patterns of the synthesized samples were performed by Rigaku MiniFlex 600 diffractometer which was equipped with an NaI:Tl scintillation detector and Ni-filtered Cu-K(α) radiation source ($\lambda = 1.54151 \text{ \AA}$). The X-ray diffraction patterns were measured in the 2θ range of 23–75° with a step of 0.02° and a scanning speed of 2°/min. Collected XRD patterns were compared to the records in the ICDD PDF-2 database (version 2013).

The top-view scanning electron microscope (SEM) images were obtained by ultra-high resolution SEM MAIA3 from TESCAN Brno with and an in-lens secondary electron detector. An electron energy of 10 keV and magnification of 50,000 was used. All samples were in their pristine state without any conductive coating.

Photoluminescence spectra were collected using a pulsed UV LED excitation source with a frequency of 333 Hz, wavelength of 340 nm and power of 1 mW. The excitation source was additionally filtered by a narrow band-pass filter centered at 340 nm. The PL spectra were obtained using a double-grating monochromator SPEX 1672 with 2 nm spectral resolution, a photomultiplier sensitive in the 350–750 nm cooled by the Peltier effect, and a lock-in amplifier referenced to the frequency of excitation LED. The measured samples were prepared by pressing 5 mg of BaI₂:Eu/GNP powder into a pellets with a diameter of 3 mm which were further attached to the holder by double-sided conductive tape. All measurements were provided in a vacuum using an Oxford Instruments OptistatDry BLV cryostat. The data were converted from wavelength to energy scale using Jacobian correction [33].

The PL decay times were measured for all samples for a 3 eV emission band under excitation by nanoLED at 3.66 eV (339 nm). In order to determine true decay times, the deconvolution procedure (SpectraSolve software package, Ames Photonics) was applied to the decay curves.

Radioluminescence (RL) spectra measurements at room temperature (290 K) were performed by the Horiba Jobin-Yvon 5000 M spectrometer, TBX-04 (IBH) photomultiplier operating in the 200–800 nm spectral range and monochromator with a spectral resolution of 8 nm. The samples were irradiated by a Seifert X-ray tube operated at 40 kV with a tungsten target. All the spectra were corrected for experimental distortions caused by the setup.

Electron paramagnetic resonance (EPR) spectra measurements were obtained at room temperature (290 K) using a commercial Bruker EMXplus spectrometer in the X-band (9.4 GHz). The spectrometer sensitivity is about 10¹² spins/mT, while microwave power of 1–2 mW, modulation amplitude of 0.1–0.5 mT and time constant of 160 μ s were used.

3. Results and Discussion

3.1. Structural Analysis and Morphology of $BaI_2:Eu/GNP$

To verify the purity of phase BaI_2 the XRD patterns of the samples Au0, 001, 005 and 02 were measured. By comparing measured data shown in Figure 1 with the PDF database record #73–1849, one can see that, as well as containing prevailing reflections corresponding to $BaI_2 \cdot H_2O$, the XRD patterns also contain peaks of pure BaI_2 phase in the Au0 and Au001 samples. They are absent in the Au005 and Au02 samples. This may indicate the hydrophilic action of the golden nanoparticles. The $BaI_2 \cdot H_2O$ phase appears due to the hygroscopic nature of BaI_2 , particularly due to absorption of water vapor released during synthesis or air moisture (see Equation (1)). The unit cell parameters and coherent scattering region (CSR) standing for the size of the BaI_2 crystallites were calculated for $BaI_2 \cdot H_2O$ phase. The unit cell parameters, together with crystallite sizes of the samples Au0, 001, 005 and 02, are given in Table 2. Note that the calculated values of the unit cell parameters are in accordance with the PDF database record #39–1300 for the $BaI_2 \cdot H_2O$ phase.

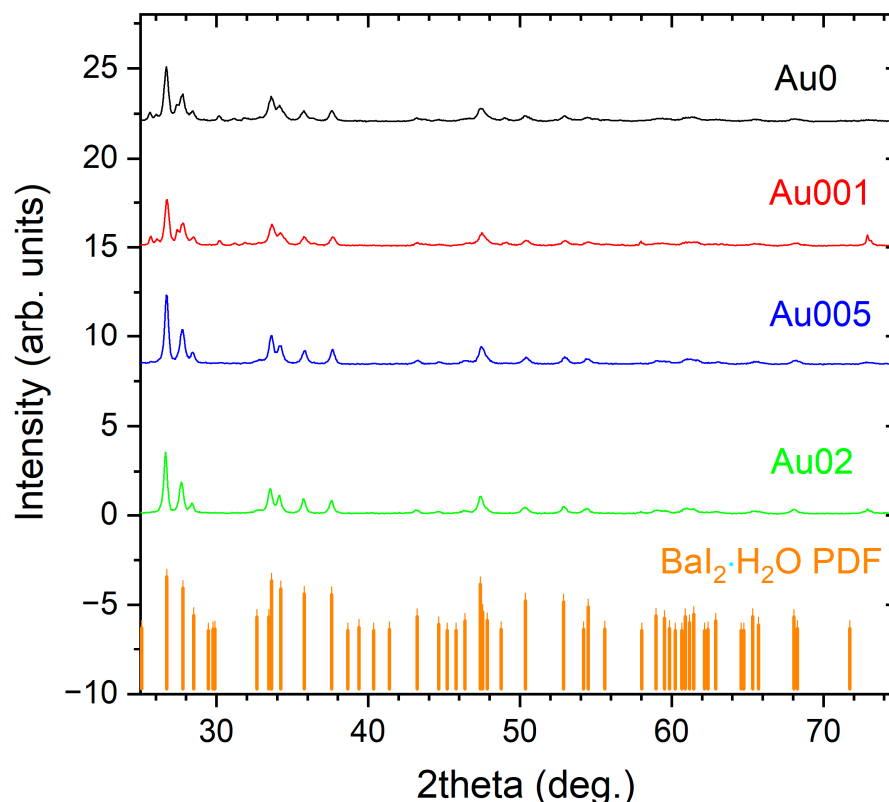


Figure 1. XRD patterns of the $BaI_2:Eu/GNP$ samples (see Table 1) together with database patterns PDF #39–1300 corresponding to $BaI_2 \cdot H_2O$ phase.

Table 2. Unit cell parameters and crystallites size of the Eu doped $BaI_2 \cdot H_2O/GNP$ samples (see Table 1).

| Sample | a (Å) | b (Å) | c (Å) |
|--------|--------------------|-------------------|--------------------|
| Au0 | 12.507 ± 0.003 | 4.768 ± 0.003 | 10.010 ± 0.003 |
| Au001 | 12.508 ± 0.003 | 4.767 ± 0.003 | 10.009 ± 0.003 |
| Au005 | 12.509 ± 0.003 | 4.768 ± 0.003 | 10.008 ± 0.003 |
| Au02 | 12.517 ± 0.003 | 4.772 ± 0.003 | 10.012 ± 0.003 |

The obtained lattice parameters are in a good agreement with the previously reported in [34].

The incorporation of GNPs into BaI₂:Eu leads to the fluctuations in the unit cell parameters, as can be seen from Table 2. This may indicate the presence of two competing processes. A slight decrease of the lattice parameter *c* upon the rising GNP content from 0 to 0.005% (see Table 1) and fluctuation of the parameter *b*, may be caused by substitution of smaller Au⁺ or Au³⁺ for larger Ba²⁺ ions in BaI₂ [35]. The ionic radii of Au⁺, Au³⁺ and Ba²⁺ are 1.37 Å, 0.68 Å and 1.47 Å, respectively. The formation of compounds, such as AuI, AuI₂[−] and AuI₄[−] [36–38] during the synthesis may also explain the decrease of cell volumes upon GNP co-doping. However, these material phases were not detected in the XRD patterns (Figure 1). On the contrary, the slight increases of unit cell parameters upon co-doping with GNP, which is most obvious for the unit cell parameter *a* (all concentrations studied) and *b* (for the concentration 0.2%), may be explained by the incorporation of Au particles into the lattice in the interstitial positions.

3.2. Luminescence and Timing Characteristics

The PL spectra of the samples Au0, 001, 005 and 02 measured at 290 K are shown in Figure 2a. The main PL bands are narrow and almost symmetric with the maximum at about 3 eV (Figure 2a). They were related to the Eu²⁺ 4f⁶5d¹ → 4f⁷ transition in BaI₂ [19,39]. Another “tail”-like band in the 2.2–2.8 eV region can be visible for all the samples (Figure 2a). To attain higher resolution of the PL spectra, they were also measured at 10 K (Figure 2b). Now, the unresolved broad band at 2.2–2.8 eV becomes the low-intensity bands with the maxima at 2.36 eV and 2.76 eV, respectively. These are most visible in PL spectra of Au0 at 10 K and are almost absent in the Au001, 005 and 02 samples at room temperature (Figure 2). The total intensity of secondary PL bands between 2.2–2.8 eV does not change significantly with temperature (Figure 2). This indicates weak coupling of the corresponding emission centers with the lattice. It is worth mentioning that similar double-peak structured bands have also been recorded in undoped BaCl₂ and BaBr₂ where they were related to H and F centers [17]. However, the exact origin of the bands in the present case is unknown and requires extended study which is beyond the subject addressed in the present paper and will be considered elsewhere.

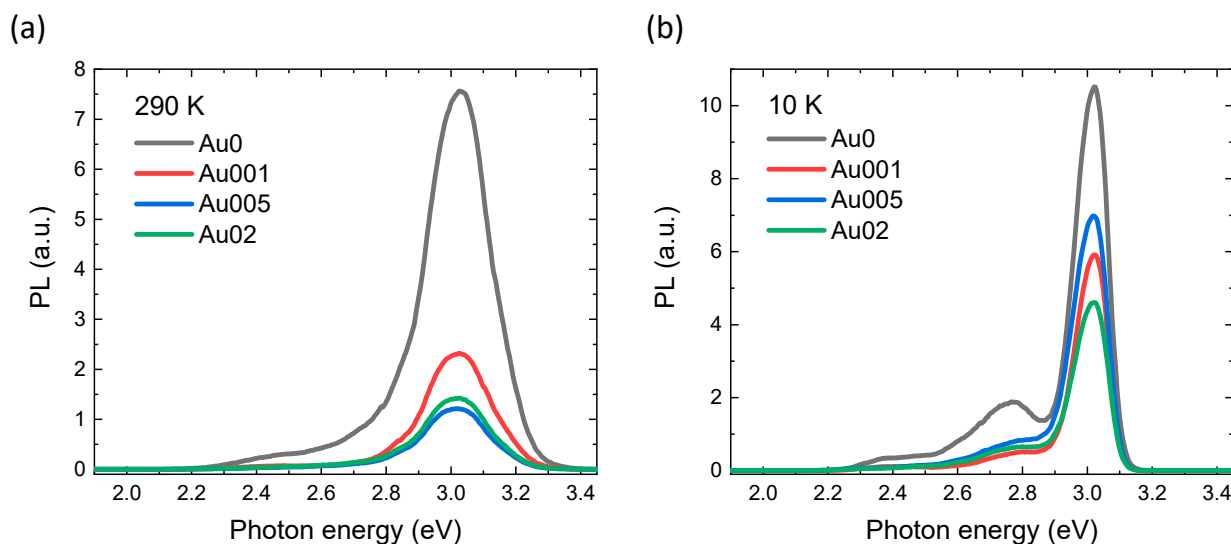


Figure 2. Photoluminescence spectra for the BaI₂:Eu/GNP samples measured at (a) room temperature 290 K and (b) 10 K.

The Eu²⁺ band is narrowing and its amplitude is increased only slightly with the temperature lowering (Figure 2b). This again indicates a weak bonding of the Eu²⁺ to ligand iodine anions.

As can be seen in Figure 2, the GNP co-doping significantly affects the luminescence properties of the BaI₂:Eu samples. The PL band of the Eu²⁺ generally decreases with GNP

content. Comparing the main PL bands at 3 eV, a 2.3-fold decrease in the PL maximum intensity of sample Au02 compared to sample A0 was observed at 10 K. A deteriorated luminescence of the main peak corresponding to Eu^{2+} upon GNP co-doping may be explained by the Au^+ incorporation competing with the incorporation of Eu^{2+} . The PL intensities of both secondary bands at 2.76 eV and 2.36 eV of Au02 sample decrease more significantly by factor 3 and 5.3, respectively, compared to Au0 sample at 10 K. The Au^+ ions may be incorporated into the lattice in interstitial positions, thereby supplying additional positive charge to the system. Thanks to charge compensation, the presence of the extra positively charged Au interstitials suppresses the formation of the corresponding emission centers.

PL decay kinetics was further measured in all samples at 420 nm (3 eV), which corresponds to the emission maximum of the Eu^{2+} . The decay curve of the sample Au02 together with the fit obtained using the standard single-exponential approach and deconvolution procedure are depicted in Figure 3. The decay curves of other samples show qualitatively similar trends. The obtained decay times from the individual fits are in the order of hundreds of nanoseconds and are listed in Table 3. It is seen that the decay time is shortening with the increasing concentration of GNPs. Strong concentration effect of the GNPs on the Eu^{2+} luminescence properties of the $\text{BaI}_2:\text{Eu}$ samples is clearly observed. This can be explained by the Richardson–Schottky effect coupled with the plasmonic Au nanoparticles [30,31]. The incident 340 nm light (3.88 eV) moderates negative charge (electron) density in the golden nanoparticles at the GNP/ BaI_2 interface and beyond it in the BaI_2 crystallite itself. This extra negative charge appeared next to the excited Eu^{2+} having the excited $5d^1$ level. The repulsion appearing in this place forces the electron in the excited state to relax to the stable ground state. Therefore, GNPs speed up the luminescence. The larger the amount of Au nanoparticles, the stronger the influence. As a result, the Eu^{2+} decay time decreases with the doping level of golden particles. However, since the number of Au nanoparticles is, in general, small (not more than 0.2%, see Table 1) and, taking into account that the overall europium doping level is 5% (note, that not all Eu^{2+} ions of the total 5% are in the excited state) the effect is weak (Table 3).

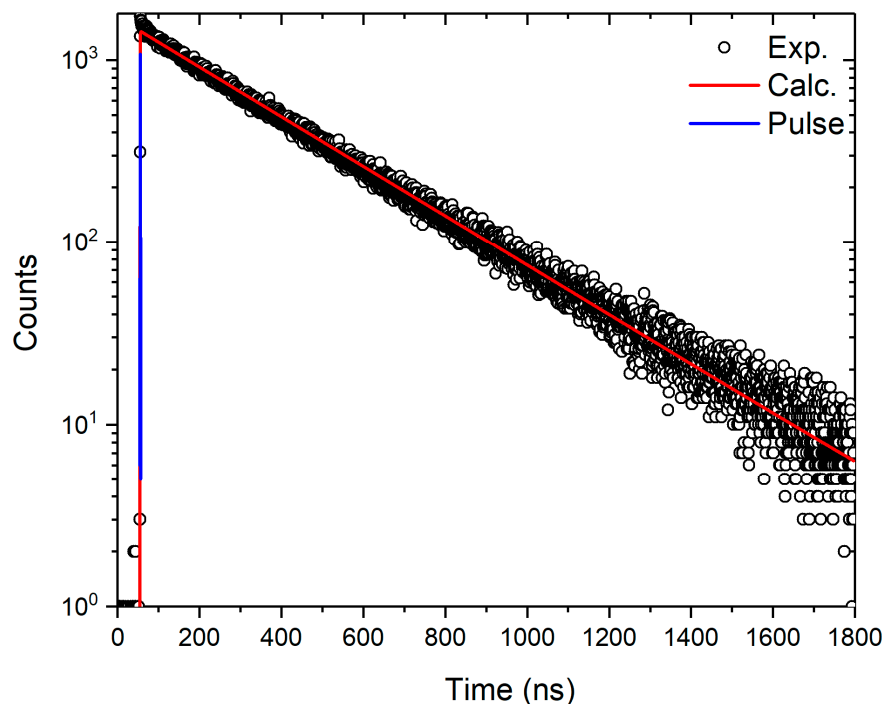
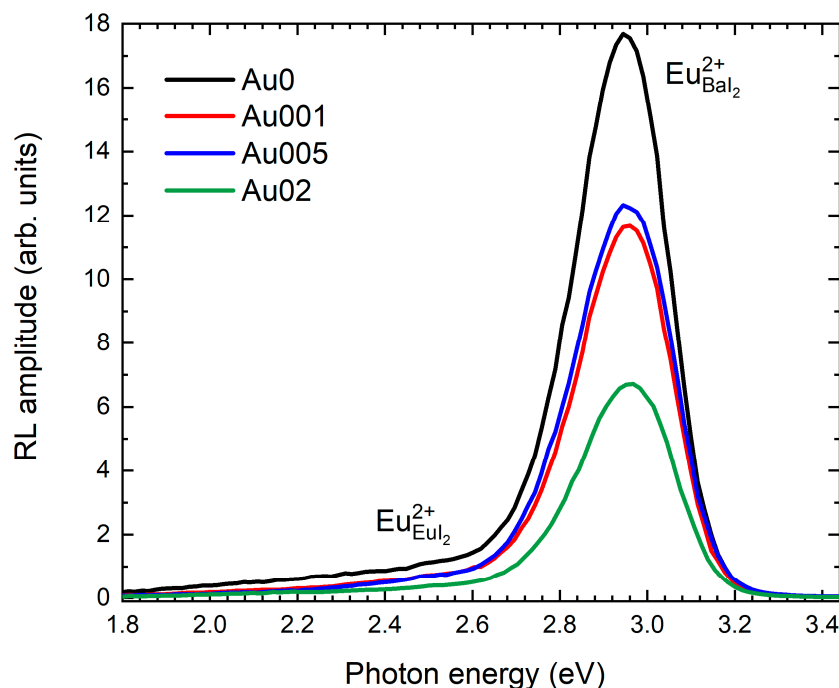


Figure 3. PL experimental and fitted decay curves measured on $\text{BaI}_2:\text{Eu}$ with GNP (sample Au02).

Table 3. PL decay time constants for the Eu^{2+} band peaking at 420 nm (3 eV).

| Sample | Decay Time (ns) |
|--------|-----------------|
| Au0 | 324.8 ± 0.2 |
| Au001 | 322.5 ± 0.2 |
| Au005 | 322.6 ± 0.2 |
| Au02 | 318.8 ± 0.2 |

To investigate the characteristics of scintillation performance, a room temperature radioluminescence was measured in all the samples. The spectra are shown in Figure 4.

**Figure 4.** RL spectra of the samples at 295 K.

The RL spectra are composed of the two signals: dominating band peaking at 2.9 eV attributed to Eu^{2+} in BaI_2 and the weaker band within the ~ 1.8 – 2.7 eV range attributed to Eu^{2+} in EuI_2 based on previous work [19] (Figure 4). The spectral positions of these bands do not depend on the GNP content while their intensities are decreasing. This correlates strongly with PL spectra measurements in Figure 2. The band intensities of the samples Au001 and Au005 are almost the same and about 1.4 times weaker as compared to the Au0 sample. The intensity of the A02 sample is about 2.6 times weaker as compared to the Au0 sample. To gain better insight into these peculiarities, EPR was measured.

3.3. Eu^{2+} Incorporation by EPR

EPR spectra measured on the Au0, 001, 005 and 02 samples are shown in Figure 5. Considering only one cation, Ba^{2+} with ionic radius 1.38 \AA , the most probable localization of the Eu^{2+} with ionic radius 1.2 \AA in the lattice is Ba^{2+} site (D_{2d} local symmetry [34]). Both ionic radii were taken from [35] for the ligand coordination 7. A multi-feature Eu^{2+} EPR spectrum in Figure 5 indicates the Eu^{2+} localization at the regular site due to strong interaction with ligands (relatively strong ligand field) [40]. Detailed justification of the Eu^{2+} localization in the BaI_2 host is provided in [19].

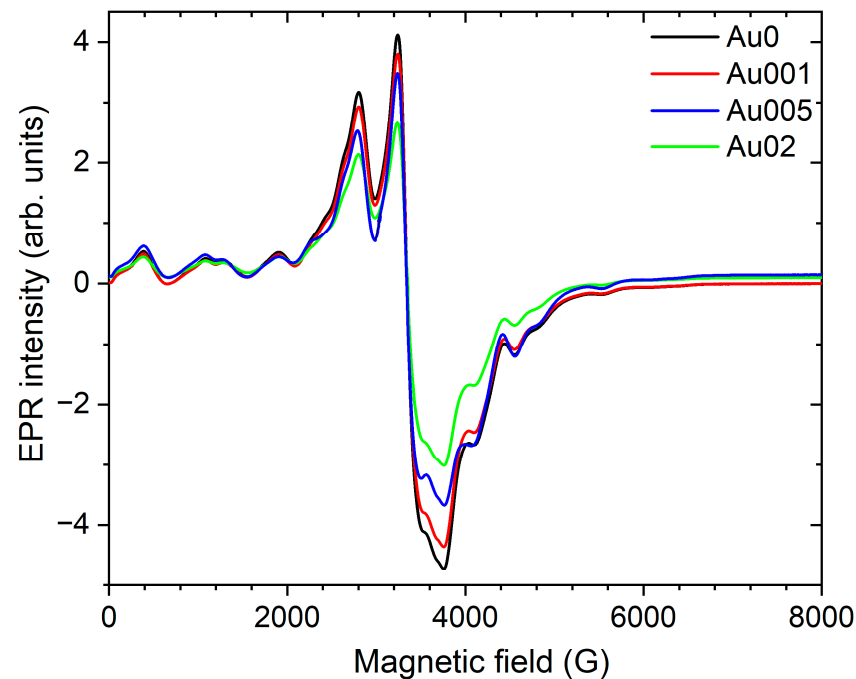


Figure 5. EPR spectra of the BaI₂:Eu/GNP samples (see Table 1).

The intensity of the Eu²⁺ EPR spectrum reduces with GNP content (Figure 5). This agrees well with the trends observed for the strongly dominating 3 eV PL and 2.9 eV RL bands (Figures 2 and 4). Therefore, one can unambiguously refer these bands to the Eu²⁺ at Ba²⁺ site. This can be explained as follows. The incorporation of Au into the BaI₂ grains instead of barium as Au_{Ba}⁻ creates concurrence for the Eu²⁺ substitution. In this case extra negative charge is created which should be compensated in the way Eu_{Ba}⁺ = Au_{Ba}⁻ which increases the concentration of Eu³⁺ ions. However, the PL or RL Eu³⁺ spectra were not detected (Figures 2 and 4) and, therefore, the creation of the EuI₂ phase is possible. This agrees with the red-energy shoulder existing in both RL and PL spectra (Figures 2 and 4). However, the EPR signals of the EuI₂ cannot be detected due to the strong resonance line broadening, which occurs because of close packing of Eu²⁺ ions in the EuI₂ [40].

4. Conclusions

The properties of BaI₂:Eu (5 at.%) nanocrystalline powders decorated with varying content of gold nanoparticles are studied with emphasis on Eu²⁺ incorporation. The XRD patterns show simultaneous existence of the BaI₂ and BaI₂·H₂O phases due to the hygroscopic nature of BaI₂. The slight fluctuations in the BaI₂ unit cell parameters upon GNP decoration corresponded to two competing processes. The decrease of the *c* parameter particularly results from the substitution of smaller Au⁺ or Au³⁺ ions for larger Ba²⁺ ions in BaI₂. The increase of the *a* parameter was explained by the incorporation of Au particles into the lattice in the interstitial positions. The PL and RL spectra consisted of the dominating emission band at about 2.9–3 eV originating from Eu²⁺ at the Ba site in the BaI₂ structure. There were also secondary broad strongly overlapped bands (2.2–2.7 eV) related to some defects whose exact origin remain unknown. GNPs present in the samples suppressed both Eu²⁺ and defect-related PL and RL. Along with the EPR measurements, this provided evidence for the degraded Eu incorporation into the BaI₂ host upon GNPs decoration. Interestingly, the PL decays were single exponential. They exhibited a decrease in the decay time of the Eu²⁺ emission according to GNP content. This is the result of the extra negative charge moderation in the GNP leading to repulsion between this negative charge and an electron in the excited state of Eu²⁺.

Author Contributions: Validation, M.B.; formal analysis, K.R., M.B., V.B., D.J., N.N., T.S., J.D. and Y.T.; investigation K.R., M.B., V.B., D.J., N.N., T.S., J.D. and Y.T.; data curation, M.B.; writing—original draft preparation, K.R., M.B., V.B., D.J., N.N., T.S., J.D. and Y.T.; writing—review and editing, M.B. and V.B.; visualization, K.R., V.B., D.J., N.N., T.S., J.D. and Y.T.; supervision, M.B.; project administration, M.B. All authors have read and agreed to the published version of the manuscript.

Funding: Mobility project “Development and enhancement of luminescent materials for multipurpose applications” of Czech Academy of Sciences and National Academy of Sciences of Belarus (No. NASB-20-03).

Data Availability Statement: Not applicable.

Acknowledgments: This work was supported by mobility project “Development and enhancement of luminescent materials for multipurpose applications” of Czech Academy of Sciences and National Academy of Sciences of Belarus (No. NASB-20-03).

Conflicts of Interest: The authors declare no conflict of interest.

References

- Feldmann, C.; Jüstel, T.; Ronda, C.; Schmidt, P. Inorganic Luminescent Materials: 100 Years of Research and Application. *Adv. Funct. Mater.* **2003**, *13*, 511–516. [[CrossRef](#)]
- Lenus, A.J.; Sornadurai, D.; Rajan, K.G.; Purniah, B. Luminescence behaviour of Eu²⁺-doped BaClI and BaBrI. *Mater. Lett.* **2002**, *57*, 635–638. [[CrossRef](#)]
- Terraschke, H.; Wickleder, C. UV, Blue, Green, Yellow, Red, and Small: Newest Developments on Eu²⁺-Doped Nanophosphors. *Chem. Rev.* **2015**, *115*, 11352–11378. [[CrossRef](#)] [[PubMed](#)]
- Shendrik, R.; Shalaev, A.; Myasnikova, A.; Bogdanov, A.; Kaneva, E.; Rusakov, A.; Vasilkovskiy, A. Optical and structural properties of Eu²⁺ doped BaBrI and BaClI crystals. *J. Lumin.* **2017**, *192*, 653–660. [[CrossRef](#)]
- Pankratov, V.; Popov, A.; Shirmane, L.; Kotlov, A.; Bizarri, G.; Burger, A.; Bhattacharya, P.; Tupitsyn, E.; Rowe, E.; Buliga, V.; et al. Luminescence and ultraviolet excitation spectroscopy of SrI₂ and SrI₂:Eu²⁺. *Radiat. Meas.* **2013**, *56*, 13–17. [[CrossRef](#)]
- Ramanantoanina, H.; Merzoud, L.; Muya, J.T.; Chermette, H.; Daul, C. Electronic Structure and Photoluminescence Properties of Eu(η⁹-C₉H₉)₂. *J. Phys. Chem. A* **2020**, *124*, 152–164. [[CrossRef](#)]
- Cherepy, N.J.; Hull, G.; Niedermayr, T.R.; Drobshoff, A.; Payne, S.A.; Roy, U.N.; Cui, Y.; Bhattacharaya, A.; Harrison, M.; Guo, M.; et al. Barium iodide single-crystal scintillator detectors. *Hard X-Ray Gamma-Ray Detect. Phys. IX* **2007**, 6706, 670616. [[CrossRef](#)]
- Nikl, M. (Ed.) *Nanocomposite Ceramic and Thin Film Scintillators*; Pan Stanford Publishing Pte. Ltd.: Singapore, 2017.
- Biswas, K.; Sontakke, A.; Sen, R.; Annapurna, K. Luminescence Properties of Dual Valence Eu Doped Nano-crystalline BaF₂ Embedded Glass-ceramics and Observation of Eu²⁺ → Eu³⁺ Energy Transfer. *J. Fluoresc.* **2012**, *22*, 745–752. [[CrossRef](#)]
- Tratsiak, Y.; Buryi, M.; Babin, V.; Korjik, M.; Trusova, E. The effect of binary glass composition on the Eu-ions luminescence properties. *Opt. Mater.* **2019**, *94*, 356–362. [[CrossRef](#)]
- Gahane, D.; Kokode, N.; Muthal, P.; Dhopte, S.; Moharil, S. Luminescence of Eu²⁺ in some iodides. *Opt. Mater.* **2009**, *32*, 18–21. [[CrossRef](#)]
- Kalpana, T.; Brik, M.; Sudarsan, V.; Naresh, P.; Kumar, V.R.; Kityk, I.; Veeraiiah, N. Influence of Al³⁺ ions on luminescence efficiency of Eu³⁺ ions in barium boro-phosphate glasses. *J. Non-Crystalline Solids* **2015**, *419*, 75–81. [[CrossRef](#)]
- Dejneka, M.; Snitzer, E.; Riman, R. Blue, green and red fluorescence and energy transfer of Eu³⁺ in fluoride glasses. *J. Lumin.* **1995**, *65*, 227–245. [[CrossRef](#)]
- Liu, X.; Lin, C.; Lin, J. White light emission from Eu³⁺ in CaIn₂O₄ host lattices. *Appl. Phys. Lett.* **2007**, *90*, 081904. [[CrossRef](#)]
- Xie, H.; Lu, J.; Guan, Y.; Huang, Y.; Wei, D.; Seo, H.J. ChemInform Abstract: Abnormal Reduction, Eu³⁺ → Eu²⁺, and Defect Centers in Eu³⁺-Doped Pollucite, CsAlSi₂O₆, Prepared in an Oxidizing Atmosphere. *Cheminform* **2014**, *45*, 827–834. [[CrossRef](#)]
- Zhai, Y.; You, Z.; Liu, Y.; Sun, Y.; Ji, Q. Properties of red-emitting phosphors Sr₂MgSi₂O₇:Eu³⁺ prepared by gel-combustion method assisted by microwave. *J. Rare Earths* **2012**, *30*, 114–117. [[CrossRef](#)]
- Selling, J.; Birowosuto, M.D.; Dorenbos, P.; Schweizer, S. Europium-doped barium halide scintillators for x-ray and γ-ray detections. *J. Appl. Phys.* **2007**, *101*, 034901. [[CrossRef](#)]
- Tret'yak, E.V.; Shevchenko, G.P.; Solomakha, T.A.; Korzhik, M.V. Effect of precursor morphology on the structural properties, optical absorption, and luminescence of BaI₂:Eu²⁺, Eu³⁺. *Inorg. Mater.* **2017**, *53*, 307–312. [[CrossRef](#)]
- Salamakha, T.; Buryi, M.; Tratsiak, Y. Effect of Eu-doping on optical, structural and morphological properties of BaI₂·nH₂O powders. *Opt. Mater.* **2018**, *78*, 352–359. [[CrossRef](#)]
- Pejchal, J.; Buryi, M.; Babin, V.; Prusa, P.; Beitlerova, A.; Barta, J.; Havlak, L.; Kamada, K.; Yoshikawa, A.; Laguta, V.; et al. Luminescence and scintillation properties of Mg-codoped LuAG:Pr single crystals annealed in air. *J. Lumin.* **2017**, *181*, 277–285. [[CrossRef](#)]
- Chen, Y.; Yang, H.K.; Park, S.W.; Moon, B.K.; Choi, B.C.; Jeong, J.H.; Kim, K.H. Characterization and photoluminescent enhancement of Li⁺ corporation effect on CaWO₄:Eu³⁺ phosphor. *J. Alloy. Compd.* **2012**, *511*, 123–128. [[CrossRef](#)]

22. Liu, D.; Shi, J.; Tong, L.; Ren, X.; Li, Q.; Yang, H. YVO₄:Eu³⁺, Dy³⁺@Fe₃O₄ co-doped nanocomposites: Preparation, luminescent, and magnetic properties. *J. Nanoparticle Res.* **2012**, *14*, 1216. [[CrossRef](#)]
23. Zhou, H.; Wu, G.; Qin, N.; Bao, D. Dual Enhancement of Photoluminescence and Ferroelectric Polarization in Pr³⁺/La³⁺-Codoped Bismuth Titanate Thin Films. *J. Am. Ceram. Soc.* **2010**, *93*, 2109–2112. [[CrossRef](#)]
24. Shalapska, T.; Moretti, F.; Bourret, E.; Bizarri, G. Effect of Au codoping on the scintillation properties of BaBrCl:Eu single crystals. *J. Lumin.* **2018**, *202*, 497–501. [[CrossRef](#)]
25. Levchenko, V. Luminescence of Europium complex enhanced by surface plasmons of gold nanoparticles for possible application in luminescent solar concentrators. *J. Lumin.* **2018**, *193*, 5–9. [[CrossRef](#)]
26. Malashkevich, G.E.; Chukova, O.V.; Nedilko, S.G.; Shevchenko, G.P.; Bokshyts, Y.V.; Kouhar, V.V. Influence of Gold Nanoparticles on Luminescence of Eu³⁺ Ions Sensitized by Structural Defects in Germanate Films. *J. Phys. Chem. C* **2016**, *120*, 15369–15377. [[CrossRef](#)]
27. Wackerow, S.; Seifert, G. Co-doping of glasses with rare earth ions and metallic nanoparticles for frequency up-conversion. *Photonics Sol. Energy Syst. III* **2010**, 7725, 77251H. [[CrossRef](#)]
28. Hussain, T.; Zhong, L.; Danesh, M.; Ye, H.; Liang, Z.; Xiao, D.; Qiu, C.-W.; Lou, C.; Chi, L.; Jiang, L. Enabling low amounts of YAG:Ce³⁺ to convert blue into white light with plasmonic Au nanoparticles. *Nanoscale* **2015**, *7*, 10350–10356. [[CrossRef](#)]
29. Kahane, S.V.; Sudarsan, V.; Mahamuni, S. A study of charge transfer mechanism and optical properties of Au–CdS core–shell nanocrystals. *J. Lumin.* **2014**, *147*, 353–357. [[CrossRef](#)]
30. Emtage, P.R.; O'Dwyer, J.J. Richardson-Schottky Effect in Insulators. *Phys. Rev. Lett.* **1966**, *16*, 356–358. [[CrossRef](#)]
31. Moores, A.; Goettmann, F. The plasmon band in noble metal nanoparticles: An introduction to theory and applications. *New J. Chem.* **2006**, *30*, 1121–1132. [[CrossRef](#)]
32. Salamakha, T.; Trusova, E.E.; Tratsiak, Y.U. Preparation and study of the luminescent glass-ceramics based on barium iodide activated with Eu²⁺. *J. Belarusian State Univ. Chem.* **2019**, *1*, 38–44. [[CrossRef](#)]
33. Mooney, J.; Kambhampati, P. Get the Basics Right: Jacobian Conversion of Wavelength and Energy Scales for Quantitative Analysis of Emission Spectra. *J. Phys. Chem. Lett.* **2013**, *4*, 3316–3318. [[CrossRef](#)]
34. Lutz, H.D.; Buchmeier, W.; Engelen, B. Comparative study of the crystal structures of isotypic MX₂·H₂O, M = Sr, Ba, and X = Cl, Br, I. Bifurcated H bonds in solid hydrates. *Acta Cryst.* **1987**, *B43*, 71–75. [[CrossRef](#)]
35. Shannon, R.D. Revised effective ionic radii and systematic studies of interatomic distances in halides and chalcogenides. *Acta Crystallogr. Sect.* **1976**, *A32*, 751–766. [[CrossRef](#)]
36. Davis, A.; Tran, T.; Young, D. Solution chemistry of iodide leaching of gold. *Hydrometallurgy* **1993**, *32*, 143–159. [[CrossRef](#)]
37. Davis, A.; Tran, T. Gold dissolution in iodide electrolytes. *Hydrometallurgy* **1991**, *26*, 163–177. [[CrossRef](#)]
38. Elding, L.I.; Skibsted, L.H. Kinetics and mechanism for reduction of ammine and haloammine complexes of gold(III) by iodide. *Inorg. Chem.* **1986**, *25*, 4084–4087. [[CrossRef](#)]
39. Yan, Z.; Gundiah, G.; Bizarri, G.A.; Samulon, E.C.; Derenzo, S.E.; Bourret-Courchesne, E.D. Eu²⁺-activated BaCl₂, BaBr₂ and BaI₂ scintillators revisited. *Nucl. Instruments Methods Phys. Res. Sect. A Accel. Spectrometers, Detect. Assoc. Equip.* **2014**, *735*, 83–87. [[CrossRef](#)]
40. Abragam, A.; Bleaney, B. *Electron Paramagnetic Resonance of Transition Ions*; Oxford University Press: Oxford, UK, 2012.

Disclaimer/Publisher's Note: The statements, opinions and data contained in all publications are solely those of the individual author(s) and contributor(s) and not of MDPI and/or the editor(s). MDPI and/or the editor(s) disclaim responsibility for any injury to people or property resulting from any ideas, methods, instructions or products referred to in the content.